Composites Research

Vol. 29, No. 4, 179-185 (2016)
DOI: http://dx.doi.org/10.7234/composres.2016.29.4.179
ISSN 2288-2103(Print), ISSN 2288-2111(Online)

Special Issue Paper

Self Charging Sulfanilic Acid Azocromotrop/Reduced Graphene Oxide Decorated Nickel Oxide/Iron Oxide Solar Supercapacitor for Energy Storage Application

Sanjit Saha*, Milan Jana*, Pranab Samanta*, Naresh Chandra Murmu*, Joong Hee Lee, Tapas Kuila*†**

ABSTRACT: A self-charging supercapacitor is constructed through simple integration of the energy storage and photo exited materials at the photo electrode. The large band gap of NiO/Fe_3O_4 heterostructure generates photo electron at the photo electrode and store the charges through redox mechanism at the counter electrode. Sulfanilic acid azocromotrop/reduced graphene oxide layer at the photo electrode trapped the photo generated hole and store the charge by forming double layer. The solar supercapacitor device is charged within 400 s up to 0.5 V and exhibited a high specific capacitance of ~908 F/g against 1.5 A/g load. The solar illuminated supercapacitor shows a high energy and power density of 33.4 Wh/kg and 385 W/kg along with a very low relaxation time of ~15 ms ensuring the utility of the self charging device in the various field of energy storage and optoelectronic application.

Key Words: NiO/Fe_3O_4, SAC-RGO, Solar supercapacitor, Self-charging, Relaxation time

1. INTRODUCTION

The depletion of fossil fuels and environmental change forced the modern society to harvest energy from heat, wind, vibration, or light. The conversion of solar energy to electrical energy in particular is advantageous due to its high power density (1-2 times greater) as compared to the other alternative sources [1]. However the times of use are restricted for the solar energy. On the other hand, unless a form of energy storage is developed, power generation and power consumption needs to be matched, and often this is hard to achieve [1]. As a result to fulfil the rising demand of long term off grid power it is necessary to develop an alternative source of energy storage system which can deliver high power corresponding to high energy [1-4]. However, the combination of a rechargeable energy storage system along with a solar cell resulted additional volume and cost penalties. The integration of both the device on to a single system may be a promising solution in this regards [1,2,5,6]. Electrochemical supercapacitors (ESs) have received significant concentration as high-performance energy storage system, since they can afford high capacitance, large power density, faster charge-discharge cycles, and long life stability as compared to traditional batteries [4]. Nano materials are employed as the ES electrode materials due to the large surface area and high porosity. ESs store charges through two different mechanisms of electrochemical double layer capacitance (EDLC) and pseudocapacitance [4,7]. Generally the carbonaceous materials like graphene, reduced graphene oxide (rGO), carbon nano tube (CNT) and activated carbons are used as EDLC electrode materials. On the other hand the metal oxides and hydroxides store charges through faradic reversible reaction called pseudo capacitance [4,7]. However,

Received 16 August 2016, accepted 30 August 2016

*Surface Engineering & Tribology Division, Council of Scientific and Industrial Research-Central Mechanical Engineering Research Institute, Durgapur-713209, India
*†Surface Engineering & Tribology Division, Council of Scientific and Industrial Research-Central Mechanical Engineering Research Institute, Durgapur-713209, India, Corresponding author (E-mail: tkuila@gmail.com)
**Advanced Materials Research Institute for BIN Convergence Technology (BK Plus Global, Program), Department of BIN Convergence Technology, Chonbuk National University, Jeonju, Jeonbuk 54896, Republic of Korea

the low electrical conductivity, rate capability and life stability are the major limitation of the single-component nanomaterials. An efficient approach to improve the rate capability of metal oxide/hydroxide electrode is to develop a heterostructure through proper incorporation of one or two metal ions into their lattices [7,8]. The formation of heterostructure generates abundance structural defects which in turn produces multiple accessible electroactive sites enhancing the redox reaction [7,9]. A self-charging solar supercapacitor (SSC) system is developed where visible light is absorbed through a dye-sensitized nano crystalline film and energy is stored the within the active electrode materials. The SSC is a simply electrochemical cell where one of the electrodes is constructed by depositing the active materials on the transparent conducting plate.

2. EXPERIMENTAL

2.1 Synthesis of NiO/Fe_3O_4 and construction of solar supercapacitor

Herein in this work the photo-electrode was developed by deposition of NiO/Fe_3O_4 hetero structure and sulfanilic acid azocromotrop/reduced graphene oxide (SAC-RGO) on a fluorine-doped tin oxide (FTO) coated transparent glass-plate. NiO/Fe_3O_4 was prepared through one step hydrothermal reaction. $NiSO_4$ (~0.5 g) and $FeSO_4$ (~0.5 g) were dissolved in ~40 ml of distilled water. The solution was taken in a 100 ml Teflon lined autoclave. About 10 ml of ammonia solution was added, and the autoclave was maintained at 180°C for 6 h. The product (NiO/Fe_3O_4) was collected by vacuum filtration (with distilled water and ethanol) and dried inside a vacuum oven at 60°C. Graphene oxide (GO) was prepared by modified Hummer method and SAC-RGO layer was deposited through anodic electrodeposition. The nickel foam (NF) was deposited by NiO/Fe_3O_4 to produce the counter electrode. 6 M KOH was used as the electrolyte. Whatman filter paper (42 μm) was used as the separator.

2.2 Characterization

Transmission electron microscopy (TEM) was performed with JEOL TEM 2100 FS instrument (Japan) at 200 kV. X-ray photoelectron spectroscopy (XPS) was carried out by using a K-alpha X-ray photoelectron spectrometer, PHI 5000 Versa Probe II (ULVAC-PHI, Inc, Japan). The cyclic voltammetry (CV), galvanostatic charge-discharge and electrochemical impedance spectroscopy (EIS) were performed in a PARSTAT 4000 (Princeton Applied Research, USA) electrochemical workstation in a two electrode system.

3. RESULTS AND DISCUSSION

The TEM images of NiO/Fe_3O_4 and SAC-RGO are shown in Fig. 1a and 1b, respectively. NiO/Fe_3O_4 shows quite wrinkled

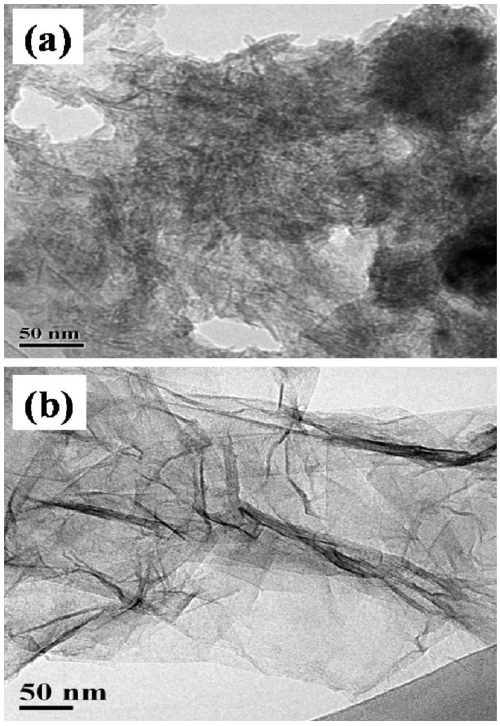

Fig. 1. TEM images of (a) NiO/Fe_3O_4 and (b) SAC-RGO

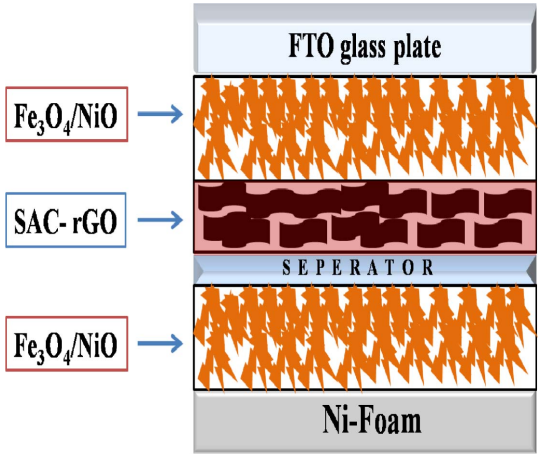

Fig. 2. Schematic representation of two electrode SSC device

arrangement with rod like particles. On the other hand, the presence of graphene sheets is clearly observed from the TEM image of SAC-RGO.

The schematic of the two electrode (SSC) is shown in Fig. 2. The formation of NiO/Fe_3O_4 heterostructure is beneficial due to the size confinement of the highly improved electron-electron interactions. Furthermore, the generation of defects or dislocations is very much expected due to the dissimilar lattice structures of the participating semiconductors and localized states are created by trapping the charge carriers of the system [7,10]. The quantum confinement effects is also reduced within the thin layers of the semiconducting heterostructure, allowing better ion exchange through the grain boundary [7,10].

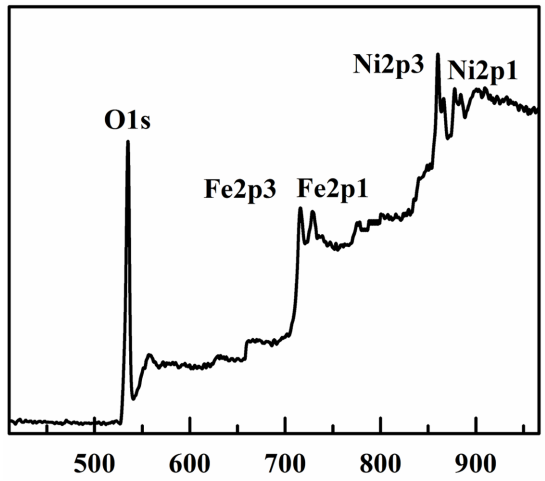

Fig. 3. XPS survey spectra of NiO/Fe_3O_4

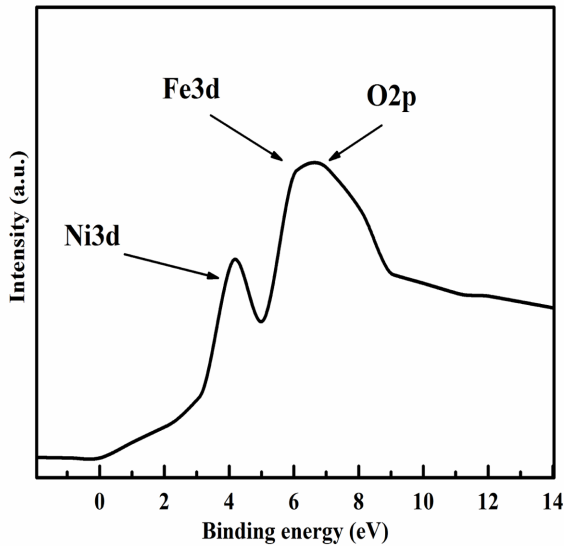

Fig. 4. XPS valance band spectra of NiO/Fe_3O_4

The appearance of two band structure creates a barrier and a quasi equilibrium potential within the electrode is established due to the confinement of the charges. Furthermore, the band alignment of heterostructures at the interface of two different materials is advantageous due to the enhanced carrier lifetimes by localizing the electron and hole within different regions of the nanostructure [11]. XPS survey spectra and the valance band spectra of NiO/Fe_3O_4 are presented in Fig. 3 and Fig. 4, respectively. The peaks at 715.1 and 728.5 eV are ascribed to the Fe 2p3/2 and Fe 2p1/2, respectively [7,12]. The peaks at 860 and 877.1 eV are ascribed to the Ni 2p3/2 and Ni 2p1/2, respectively. However, the Ni 2p3/2 position is quite dissimilar as compared to the metallic Ni (852.7 eV) [7,13]. Furthermore, the energy gap between Ni 2p3/2 and Ni 2p1/2 core levels (~17.5 eV) also different with respect to the metallic Ni (17.27 eV) [7,13]. This kind of positive shift and the amplified core

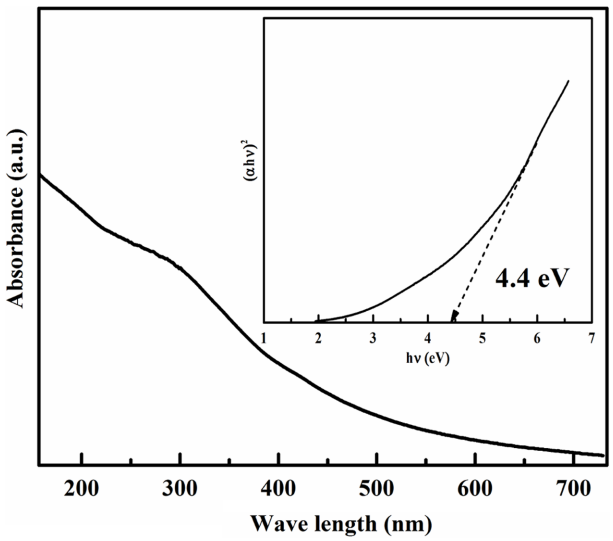

Fig. 5. UV-vis. absorption spectra of NiO/Fe_3O_4. The inset view shows the corresponding $(\alpha h\nu)^2$ vs. $h\nu$ plot

level energy difference may be due to the +2 valance state of the Ni in NiO. The valance band spectra are helpful for the detail understanding of the band structure of composite materials. The sharp peak at 4.1 eV may be attributed to the Ni3d of NiO. A broad peak is noticed around 5.8-7.3 eV. The overlapping of Fe3d and O2p peaks may be the reason of the peak broadening. It is significant to notice that the difference between the Ni3d and Fe3d peaks is more than ~1.7 eV which suggests the effective enhancement of the band gap energy due to the formation of NiO/Fe_3O_4 hetero structure.

UV-visible absorption spectroscopy was carried out to visualize the effect of the hetero structure on the optoelectronic properties of NiO/Fe_3O_4 (Fig. 5). The band structure modification of the heterostructure materials was analyzed through Tauc plot. The different position of the valance band of the metal oxides can significantly change the band structure or the band gap energy of the multi metal oxide. The appearance of broad absorption peak ~288 nm suggests the overlapping of the individual peaks related to two different metal oxides. The $(\alpha h\nu)^2$ vs. $h\nu$ plot of NiO/Fe_3O_4 is shown in the inset view of Fig. 2b. The band gap energy was measured from the intersection of the slope to the X-axis [7,14]. The band gap energy of NiO/Fe_3O_4 is ~4.4 eV which is larger than both of NiO and Fe_3O_4.

The CV of NiO/Fe_3O_4 was carried out in three electrode system using 6 M KOH electrolyte (Fig. 6a). CV shows prominent oxidation and reduction peaks at 0.35 and 0.22 V, respectively. The oxidation and reduction peak of NiO and Fe_3O_4 is appeared due to the reversible redox reaction in alkaline medium. The potential window of the NiO/Fe_3O_4 is 0.6 V (0.4-0.2 V). The specific capacitance of NiO/Fe_3O_4 was calculated from the CV following the relation

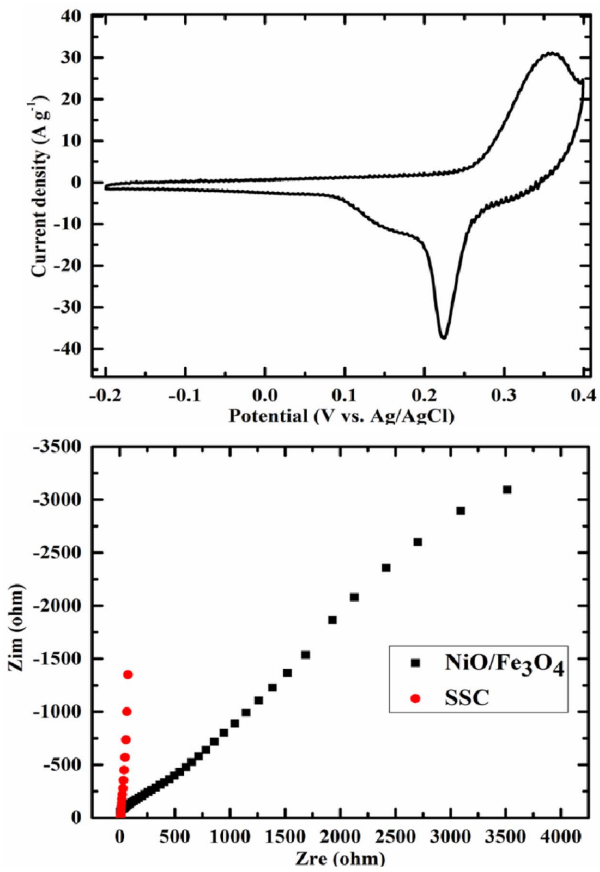

Fig. 6. (a) CV of NiO/Fe_3O_4 (b) Nyquist plot of NiO/Fe_3O_4 and SSC device

$$C_{CV} = (\int IdV)/vmV$$

where C_{CV} is the specific capacitance (F/g), I is the response current density (A /g^2), V is the potential window, υ is the scan rate (mV/s), and m is the deposited mass on the electrode. NiO/Fe_3O_4 shows very high specific capacitance of 1083 F/g at 10 mV/s scan rate. Electrochemical impedance spectroscopy (EIS) was carried out to enlighten the different charge storage mechanism of NiO/Fe_3O_4 composite and SSC devise and represented by Nyquist plot (Fig. 6b). The EIS was scanned over a frequency range of 10,000 to 0.1 Hz. The intersection of the real axis to the high frequency region is the solution resistance. The solution resistance of the NiO/Fe_3O_4 and SSC was measured as 3.5 and 4.8 ohm, respectively. The higher solution resistance may be due to the presence of additional layer of the separator and counter electrode of SSC device. However the Warburg tail of SSC is shorter and steeper as compared to the bare NiO/Fe_3O_4 electrode. The steeper Warburg suggests enhance electrical conductivity of the SSC device due to the presence of SAC-RGO layer [15]. The electrical conductivity of NiO/Fe_3O_4 and SAC-RGO was measured as 0.34 and 782 S/m respectively. Furthermore, shorter Warburg is the characteristic of the electrochemical double layer capacitance (EDLC)

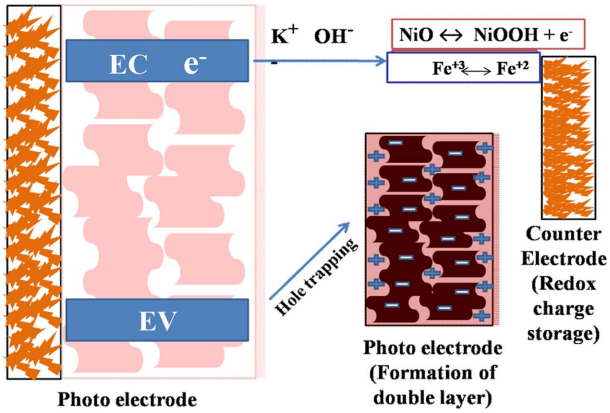

Fig. 7. Schematic representation of the charging mechanism of SSC device

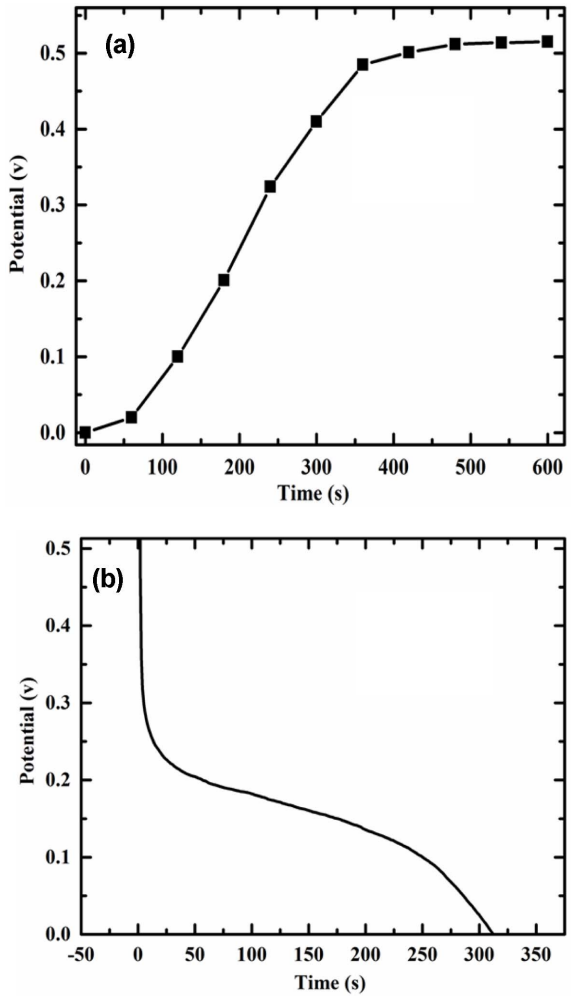

Fig. 8. (a) Charging and (b) Discharging plot of SSC device

dominated electrode materials. The presence of RGO contributed through EDLC to the SSC device and the superior electrochemical property was achieved. The elevated EIS properties also supported the good integration of the different layer of active materials, separator and electrolyte of SSC device.

Fig. 7 shows the schematic representation of the charging mechanism of SSC device. The charging process of the SSC is initiated trough a light induced photo-reaction at the NiO/Fe_3O_4 hetero junction and SAC interface. The photo exited SAC molecules cause the charge separation to the NiO/Fe_3O_4 conduction band. RGO layer plays significant role by absorbing and storing the photo generated charge through EDLC mechanism. Graphene or RGO has available free electron on the surface. The hole is trapped by SAC during the photo excitation and then stored to the RGO layer by EDLC mechanism. The photo generated electron drive the OH^- ions of the electrolyte towards the counter electrode. NiO/Fe_3O_4 can store the OH^- ions through different mechanism. The NiO store charges by following the reversible redox mechanism $NiO + OH^- \leftrightarrow NiOOH + e^-$ [7]. On the other hand Fe_3O_4 store the charge following the inter conversion between the Fe(II) and Fe(III) states [12]. It is expected that the synergistic effect of both EDLC and pseudocapacitance from RGO and NiO/Fe_3O_4 may enhance the overall electrochemical properties of the SSC device.

Fig. 8a shows the photo charging of the SSC. The photo charging initiated after ~50 s and reaches 0.5 V within 400 s. After 400 s the saturated nature is noticed during photo charging. The slope of charging profile is steeper and almost constant from 50 to 400 s. The steeper charging nature of SSC suggested fascinating charge transport through the different heterostructure and layer within the devise. The energy gained by the SSC can be measured from the discharging time up on constant. The discharging time with a constant current density gives the measurement of amount of stored charge within the cathode and anode of a supercapacitor device. It is significant to note that the SSC is able to charge itself in open circuit condition. Ultimately the SSC was eliminated up to 600 s and 0.515 V was achieved. Discharging of the SSC (without solar illumination) was carried out up on 1.5 A /g load and the discharge time was calculated as 312 s (Fig. 8b). The specific capacitance of the SSC was measured as ~908 F/g following the relation

$$C_{CD} = \frac{I\Delta t}{mV}$$

where C_{CD} is the specific capacitance (F/g), I is the discharging current (A/g^2), V is the potential window (V) and m is the deposited mass on the electrode. The energy density (E_D) and power density (P_D) of SSC also calculated according to the formula,

$$E_D = \frac{CV^2}{2} \quad \text{and} \quad P_D = \frac{E_D}{\Delta T}$$

where C is the specific capacitance, V is the operating voltage, ΔT is the discharge time. SSC is able to deliver energy of ~33.4 Wh/kg corresponding to a power density of 385 W/kg.

The charge discharge analysis shows that the as fabricated

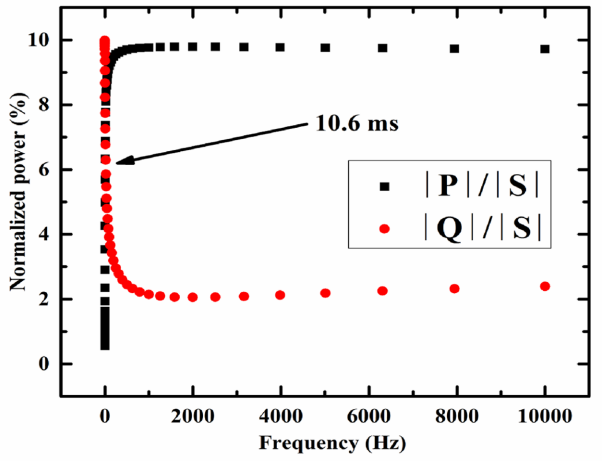

Fig. 9. Complex power plot of SSC device

SSC is able to acquire energy from the solar illumination and can deliver to a corresponding load. However the power delivery capability is another important property for an energy storage system. The relaxation time constant (τ_0) is the measurement of the efficiency of a charge storage device. The fast discharging capability or low τ_0 value is the figure of merit to evaluate the supercapacitor performance. The τ_0 may be calculated by the power dissipation analysis of the SSC device. The variation of real $P(\omega)$ and imaginary part $Q(\omega)$ of the normalized complex power $S(\omega)$ with respect to frequency scan is presented in Fig. 7. The $P(\omega)$, $Q(\omega)$ and $S(\omega)$ was measured following the relation

$$P(\omega) = \omega C''(\omega)|\Delta V_{rms}|^2$$

$$Q(\omega) = -\omega C'(\omega)|\Delta V_{rms}|^2$$

and $S(\omega) = P(\omega) + jQ(\omega)$

where j is the imaginary number. C' and C'' represent the real and imaginary part of the complex capacitance and can be calculated following the relations,

$$C'(\omega) = \frac{-Z''(\omega)}{\omega|Z(\omega)^2|}, \text{ and } C''(\omega) = \frac{Z'(\omega)}{\omega|Z(\omega)^2|}$$

.

The relaxation frequency (f_0) can be calculated from the convergence of the $P(\omega)$ and $Q(\omega)$ from the variation of real and imaginary part of the normalized complex power $S(\omega)$ as a function of frequency.

$$\text{The relaxation time constant } (\tau_0) = \frac{1}{2\pi f_0}$$

Fig. 9 shows the complex power plot of the SSC device. The f_0 of SSC device was measured as ~10.6 Hz. All the power is dissipated within the system of supercapacitor at the high frequency region where the capacitor acts like a pure resistor. On the other hand the power dissipation is almost zero at low fre-

quency.

The f_0 represents a knee value of frequency where the resistive behaviour of the supercapacitor is suppressed by capacitive behaviour. The low solution resistance of SAC-RGO as compared to the NiO/Fe_3O_4 influences the overall performance of the SSC device. Furthermore, the low τ_0 (~15 ms) indicates very fast energy delivery capability of the SSC device. The fast frequency response as well as the power delivery capacity of the SSC may be attributed to the proper integration of the layer of active materials and rich EDLC behaviour of the SAC-RGO layer of the photo electrode.

4. CONCLUSIONS

The SSC device shows proper integration of the SAC-RGO deposited NiO/Fe_3O_4 photo electrode with the NiO/Fe_3O_4 supercapacitor electrode to form a self charging and storing system. The heterostructure of the NiO/Fe_3O_4 composite plays dual role by creation of photo exited electron at the photo electrode while storing the charge by reversible redox reaction to the counter electrode. NiO/Fe_3O_4 composite shows very high specific capacitance of 1083 F/g when measured in three electrode system. SAC-RGO also serves the dual purpose. The SAC plays the role of dye by trapping the photo generated holes while the RGO adsorb the positive charge by forming the double layer with available free electrons. The charging process is performed under solar illumination at open circuit condition. The SAC-RGO and NiO/Fe_3O_4 maintains the charge balance at the photo and counter electrode respectively during the open circuit condition. The super capacitor was charged up to 0.515 V under solar illumination and exhibited high specific capacitance of 908 F g^{-1} along with energy and power density of 33.4 Wh/kg and 385 W/kg, respectively. Furthermore, the integrated device shows very low relaxation time ensuring its utility in both energy storage and optoelectronic industry.

ACKNOWLEDGEMENT

Authors are thankful to the Director of CSIR-CMERI. Authors are also thankful to the Department of Science and Technology, New Delhi, India, for the financial support from the DST-INSPIRE Faculty Scheme - INSPIRE Programme (IFA12CH-47) and Council of Scientific and Industrial Research, New Delhi, India, for funding MEGA Institutional project (ESC0112/RP-II). Also supported by Nano·Material Technology Development Program (2016M3A7B4900117) through the Ministry of Science, ICT & Future Planning, Republic of Korea.

REFERENCES

1. Chien, C., Hiralal, P., Wang, D., Huang, I., Chen, C.C., Chen, C. W., and Amaratunga, G.J., "Graphene-based Integrated Photovoltaic Energy Harvesting/storage Device," *Small,* Vol. 11, No. 24, 2015, pp. 2929-2937.
2. Miyasaka, T., and Murakami, T.N., "The Photocapacitor: An Efficient Self-charging Capacitor for Direct Storage of Solar Energy," *Applied Physics Letter,* Vol. 85, No. 17, 2004, pp. 3932-3934.
3. Li, L., Hu, Z.A., An, N., Yang, Y.Y., Li, Z.M., and Wu, H.Y., "Facile Synthesis of MnO_2/CNTs Composite for Supercapacitor Electrodes with Long Cycle Stability," *The Journal of Physical Chemistry C,* Vo. 118, No. 40, 2014, pp. 22865-22872.
4. Saha, S., Chhetri, S., Khanra, P., Samanta, P., Koo, H., Murmu, N.C., and Kuila, T., "In-situ Hydrothermal Synthesis of MnO_2/NiO@Ni Hetero Structure Electrode for Hydrogen Evolution Reaction and High Energy Asymmetric Supercapacitor Applications," *Journal of Energy Storage,* Vol. 6, 2016, pp. 22-31.
5. Wang, Z.L., "Self-powered Nanosensors and Nanosystems," *Advance Materials,* Vol. 24, No. 2, 2012, pp. 280-285.
6. Westover, A.S., Share, K., Carter, R., Cohn, A.P., Oakes, L., and Pint, C.L., "Direct Integration of a Supercapacitor into the Backside of a Silicon Photovoltaic Device," *Applied Physics Letters,* Vol. 104, 2014, pp. 213905.
7. Saha, S., Jana, M., Khanra, P., Samanta, P., Koo, H., Murmu, N. C., and Kuila, T., "Band Gap Modified Boron Doped NiO/Fe_3O_4 Nanostructure as the Positive Electrode for High Energy Asymmetric Supercapacitors," *RSC Advances*, Vol. 6, No. 2, 2016, pp. 1380-1387.
8. Dubal, P.D., Aradilla, D., Bidan, G., Gentile, P., Schubert, S.T.J., Wimberg, J., Sadki, S., and Romero, G.P., "3D Hierarchical Assembly of Ultrathin MnO_2 Nanoflakes on Silicon Nano Wires for High Performance Micro-supercapacitors in Li-doped Ionic Liquid," *Scitific Reports,* Vol. 5, 2015, pp. 09771.
9. Wang, R., and Yan, X., "Superior Asymmetric Supercapacitor Based on Ni-Co Oxide Nanosheets and Carbon Nanorods" *Scitific Reports,* Vol. 4, 2014, pp. 3712.
10. Frensley, W.R., "A Volume of VLSI Electronics: Microstructure Science," San Diego, 1994, pp. 1-28.
11. Rouhi, J., Mamat, M.H., Ooi, C.H.R., Mahmud, S., and Mahmood, M.R., "High-performance Dye-sensitized Solar Cells Based on Morphology-controllable Synthesis of ZnO-ZnS Heterostructure Nanocone Photoanodes," *Plos One*, Vol. 10, No. 4, 2015, pp.1-14.
12. Saha, S., Jana, M., Samanta, P., Murmu, N.C., Kim, N.H., Kuila T., and Lee, J.H., "Hydrothermal Synthesis of Fe_3O_4/RGO Composites and Investigation of Electrochemical Performances for Energy Storage Applications," *RSC Advances*, Vol. 4, No. 84, 2014, pp. 44777-44785.
13. Iqbal, J., Wang, B., Liu, X., Yu, D., He, B., and Yu, R., "Oxygen Vacancy Induced Green Emission and Room Temperature Ferromagnetism in Ni Doped ZnO Nanorods," *New Journal of Physics,* Vol. 11, 2009, pp. 063009.
14. Ci, L., Song, L., Jin, C., Jariwala, D., Wu, D., Li, Y., Srivastava, A., Wang, Z.F., Storr, K., Balicas, L., Liu, F., and Ajayan, P.M., "Atomic Layers of Hybridized Boron Nitride and Graphene Domains," *Nature Materials,* Vol. 9, 2010, pp. 430-435.

15. Saha, S., Jana, M., Samanta, P., Murmu, N.C., and Kuila, T., "In situ Preparation of a SAC-RGO@Ni Electrode by Electrochemical Functionalization of Reduced Graphene Oxide Using Sulfanilic Acid Azocromotrop and Its Application in Asymmetric Supercapacitors," *Journal of Materials Chemistry A,* Vol. 3, No. 38, 2015, pp. 19461-19468.
16. Ganesh, V., Pitchumani, S., and Lakshminarayanan, V., "New Symmetric and Asymmetric Supercapacitors Based on High Surface Area Porous Nickel and Activated Carbon," *Journal of Power Sources,* Vol. 158, No. 2, 2006, pp. 1523-1532.